Robust Control of a Powered Transfemoral Prosthesis Device with Experimental Verification*

Vahid Azimi[1†], Tony Shu[2], Huihua Zhao[2], Eric Ambrose[2], Aaron D. Ames[2], Dan Simon[1]

***Abstract*— This paper presents, compares, and experimentally implements two robust model-based controllers for transfemoral prosthetic walking: the robust passivity (RP) controller and the robust sliding mode (RS) controller. These findings constitute the first step toward using model-based controllers for prosthetic devices as an alternative to commonly-used variable impedance and proportional-derivative (PD) control methods. The model upon which the controllers are based is a 5-link planar hybrid system (both continuous and discrete behaviors) with point feet, to represent a transfemoral amputee's body and limbs. A desired walking trajectory is generated through the framework of human-inspired control by solving an optimization problem. Combining model and desired trajectory, a smooth humanlike gait is realized by using either controller to drive the hybrid system toward the trajectory. The stability of both resulting gaits are proven for continuous dynamics within the framework of the Lyapunov stability theorem. Simulations show the proposed controllers are capable of meeting specific performance requirements regarding robustness to force/object disturbances and trajectory tracking of the prosthetic knee while walking on flat ground. Finally, both RP and RS controllers are experimentally implemented on AMPRO3, a custom self-contained powered transfemoral prosthesis. Results show that both controllers provide humanlike walking and accurate tracking performance for a healthy human subject utilizing a transfemoral prosthesis bypass.**

I. INTRODUCTION

The number of transfemoral amputees in the United States is estimated at around 222,000 [1]. Amputees can use prosthetic legs in an attempt to restore a normal walking gait. There are three general types of prosthetic legs: passive, active, and semi-active [2]–[4]. The majority of transfemoral amputees use unactuated passive prostheses while others use semi-active prostheses capable of limited knee and/or ankle actuation. However, compared to passive and semi-active prostheses, fully actuated active prostheses can provide more stable and natural walking while simultaneously requiring less force and energy from the user [5]. The significant number of transfemoral amputees and greater efficiency of active prostheses motivate researchers to work on the design and control of powered lower-limb prostheses [6]–[8].

Variable impedance control is the most popular approach to control prostheses due to its model independency [9]–[12]. In this approach, because human walking can be considered to be cyclic gait, one step is divided into several sub-phases, and each sub-phase is controlled by its own impedance controller with corresponding impedance parameters. In general, impedance control lacks optimality and robustness due to several shortcomings: tedious impedance parameter tuning (unique to each specific amputee subject), difficulties in detecting the sub-phases during a single step, lack of feedback, and passiveness [4], [9], [13]–[15].

To address the limitations of ordinary impedance control, a prosthetic impedance controller combining a control Lyapunov function (CLF) with model independent quadratic programs (MIQP) was recently developed [16]. In [16], the proposed MIQP + impedance controller was tested on the planar 5-link bipedal robot AMBER (Advanced Mechanical Bipedal Experimental Robot) both in simulation and experiment. In [17] and [18], a nonlinear real-time optimization-based controller was designed to control AMPRO, a self-contained powered transfemoral prosthesis. The authors in [17] and [18] experimentally achieved both better tracking performance and improved energy efficiency compared to variable impedance control.

However, the aforementioned controllers are model-independent, and lack mathematical proof of stability and robustness in the presence of system uncertainties, unmodeled dynamics, and disturbances. This motivates the design of robust model-based controllers for prosthetic devices, formally guaranteeing the convergence of system error trajectories and quantitatively defining robustness to known perturbations. Importantly, such control methods need not be concerned about correct step cycle division (for switching between sub-phases) and tedious parameter tuning.

In the context of this motivation, several works have been presented on bipedal robots, rehabilitation robots, and prostheses. In [19], adaptive control of a virtual model was applied to a planar walking biped, followed by a simulation test of robustness with external disturbances. In [20], an L_1 adaptive controller was designed for a 5-link planar bipedal robot using control Lyapunov function-based quadratic programs. In [21], a control barrier function-based method inspired by a combination of backstepping, control Lyapunov functions (CLFs), and quadratic programs (QPs) was designed for bipedal robotic walking. In [22], a derivative-free Kalman filter-based (DKF) controller was designed for a powered transfemoral prosthetic test robot. In [23], four nonlinear model reference adaptive impedance controllers were tested on rehabilitation robots and haptic interfaces in both simulation and experiment.

The main contributions of this paper are twofold: (i) Quantified tracking performance and force/object disturbance robustness for two model-based robust controllers in simulated

*This work is supported by NSF Award NRI-1526519 and NSF Grant 1344954. This research was approved by the George Institute of Technology Institutional Review Board as IRB2014-0382F for testing with humans.

[1] Cleveland State University, Cleveland, OH, USA
[2] Georgia Institute of Technology, Atlanta, GA, USA
[†] Corresponding author: v.azimi@csuohio.edu

prosthetic walking, and (ii) Experimental verification of both controllers on the powered transfemoral prosthesis AMPRO3 [24], the third iteration of AMPRO, with a healthy human subject.

Our controllers only use body coordinates and able-bodied reference trajectories of the combined system without any dynamical information of the healthy body to generate prosthetic knee torque allowing the combined human-prosthesis system to emulate humanlike walking. This implies that proposed RS and RP controllers are robust not only against parameter uncertainties and unmodeled dynamics of the prosthesis part, but also for different amputee subjects.

To begin, an active transfemoral prosthesis is modeled with the prismatic-prismatic-revolute-revolute (PPRR) joint structure. This model is interfaced with a general human model to build a point prosthetic foot 5-link planar model comprised of one torso, two thighs, and two shanks as a hybrid [25] human-prosthesis system. Using able-bodied reference trajectories, an optimal smooth humanlike gait is found by solving an optimization problem. For the hybrid system and corresponding optimal gait, two different model-based robust controllers are designed: the robust sliding mode (RS) controller and the robust passivity (RP) controller.

The RS controller is designed with the aim of achieving robustness to parametric uncertainties and unmodeled dynamics (neglected dynamics and disturbances) of the human-prosthesis system. To trade off between tracking accuracy and robustness to unmodeled dynamics, a boundary layer is defined for the trajectories of the control system. The RP controller is designed to compensate for system modeling inaccuracies while providing good tracking. The RS controller's stability is proven using non-scalar boundary layer trajectories, and another proof is provided for the stability of the RP controller, both for continuous dynamics of the prosthesis system.

The proposed controllers are first verified in simulation for the human-prosthesis system and then implemented experimentally on AMPRO3 with a human test subject. Simulation results illustrate that both proposed systems have convincing tracking performance and robustness, emulating humanlike walking. Numerical results show that the RS controller outperforms the RP controller regarding robustness to push and obstacle disturbances, while the RP controller shows better tracking performance.

Both proposed controllers are then experimentally verified on AMPRO3 (using a passive ankle to simulate a point foot) with a human test subject walking for 2.5 min at a treadmill speed of 2 mph, achieving good tracking and reasonable prosthesis knee torque values for both RS and RP controllers. Experimental results echo simulation results, with the RP controller delivering better tracking performance compared to the RS controller while the RS controller generates smoother knee torque with a lower torque peak.

The paper is organized as follows: Section II describes the combined human-prosthesis system and gives an overview of human-inspired outputs and humanlike gait. Section III presents the robust controllers' structures and provides their stability analysis. Section IV presents simulation results for tracking performance and robustness to disturbances. Section V presents experimental results of both proposed controllers on AMPRO3. Section VI presents discussion, concluding remarks, and future work.

II. HUMAN-PROSTHESIS COMBINED SYSTEM

In this section, a pointed prosthetic foot 5-link planar model (one torso, two thighs, and two calves) is presented as a combined system, which includes a unified human model and transfemoral prosthetic model as shown in Fig. 1a [16].

A. Prosthesis Model

The prosthetic device (red portion in Fig. 1a) is modeled as an active transfemoral prosthesis with the PPRR joint structure as illustrated in Fig. 1b, attaching the prosthetic part to the amputee at P_a (where the socket adapter is), shown in Fig. 1a. Note that the world frame for the prosthesis system is represented as $O_o = \{x_o, y_o, z_o\}$. This prosthetic leg has four degrees of freedom: horizontal and vertical displacements of the attach point P_a, thigh angle, and knee angle. In this paper, the prosthetic ankle is assumed to be underactuated while the human side remains actuated at the ankle; the combined model can be considered as a two-domain hybrid asymmetric human-prosthesis system with one domain for human stance and the other for prosthetic stance. For an illustration of the proposed two-domain hybrid asymmetric human-prosthesis system, consider the general loop pattern in Fig. 4a.

B. Hybrid Model

Because the combined system has both continuous and discrete (instantaneous velocity changes upon impact) behaviors, the human-prosthesis bipedal structure can be considered a hybrid system [25] with configuration space Q_R in local coordinates $q_c = (q_{sf}, q_{sk}, q_{sh}, q_{nsh}, q_{nsk})^T$ and world frame defined as $O_{co} = \{x_{co}, y_{co}, z_{co}\}$, illustrated in Fig. 1a. Using the Euler-Lagrange formula, the equations of motion of the bipedal continuous dynamics [17] are given as

$$M_c(q_c)\ddot{q}_c + C_c(q_c, \dot{q}_c)\dot{q}_c + g_c(q_c) = Bu_c \qquad (1)$$

where $M_c \in \Re^{5\times5}$ is the inertia matrix; $C_c \in \Re^{5\times5}$ is the Coriolis and centripetal matrix; $g_c \in \Re^{5\times1}$ is the gravity vector; $B \in \Re^{5\times1}$ is the torque map with underactuated prosthesis side and actuated human side; u_c is the vector of torque inputs.

To emulate humanlike walking, actual combined system outputs y_a must converge to desired human outputs y_d, where actual outputs y_a are comprised of forward hip velocity, knee angles, non-stance slope, and torso angle [17], [26]. An optimal smooth humanlike gait (i.e., desired human outputs y_d) is attained by solving an optimization problem composed of able-bodied reference trajectories along with partial hybrid zero dynamics (PHZD) constraints and the canonical walking function (CWF) [26]. Desired joint angles and angular velocities of the combined system (q_c^d) are calculated using the PHZD reconstruction procedure [26].

The equations of motion of the prosthetic leg shown in Fig. 1b are derived using the Euler-Lagrange formula:

$$M_p(q_p)\ddot{q}_p + C_p(q_p, \dot{q}_p)\dot{q}_p + g_p(q_p) = u_p \tag{2}$$

where $q_p = (q_{p1}, q_{p2}, q_{p3}, q_{p4})^T$ represents the vector of generalized joint displacements of the prosthetic device (q_{p1} and q_{p2} are the horizontal and vertical displacement of the attach point P_a respectively, and q_{p3} and q_{p4} are thigh and knee angles respectively); $M_p \in \Re^{4\times4}$, $C_p \in \Re^{4\times4}$, and $g_p \in \Re^{4\times1}$ are the inertia matrix, Coriolis and centripetal matrix, and gravity vector respectively; u_p is the prosthesis control signal comprising horizontal and vertical forces at the hip and active control torques at the thigh and knee.

The scope of this paper extends to control of the prosthetic knee joint shown in Fig. 1a using the two proposed robust controllers introduced in Section III. These controllers receive input set $S_c = \{q_c, q_c^d\}$ and hip information from the combined system and healthy body. Using a linear transformation, the set $S_p = \{q_p, q_p^d\}$ is generated from S_c, where q_p^d is the desired trajectory for q_p. The controllers use S_p to generate prosthetic knee torque during both swing and stance phases, allowing the combined human-prosthesis system to emulate humanlike walking, i.e., $q_p \to q_p^d \Rightarrow q_c \to q_c^d \Rightarrow y_a \to y_d$ with bounded tracking error trajectories.

Since body coordinates are defined based on stance and non-stance phases, the fourth element of u_p is replaced by the second element of u_c when the prosthesis device is the stance leg, and likewise, the fourth element of u_p is replaced by the fifth element of u_c when the prosthesis is the non-stance leg. In this manner, the prosthesis control signal remains correctly defined during stance and non-stance phases.

III. ROBUST PROSTHESIS CONTROLLERS

This section defines two different model-based robust controllers to control the prosthesis device (i.e., prosthetic knee joint, where prosthetic ankle is underactuated), simultaneously considering the shortcomings of traditional impedance control and providing a robust and stable control structure for prosthetic walking. As both controllers are model-based, the prosthesis model depicted in Fig. 1b is used to control the prosthetic knee joint (red part) in Fig. 1a. To control the other joints and obtain stable and humanlike walking, a feedback linearization human-inspired controller is used to drive the actual outputs of the system to the desired ones exponentially [26].

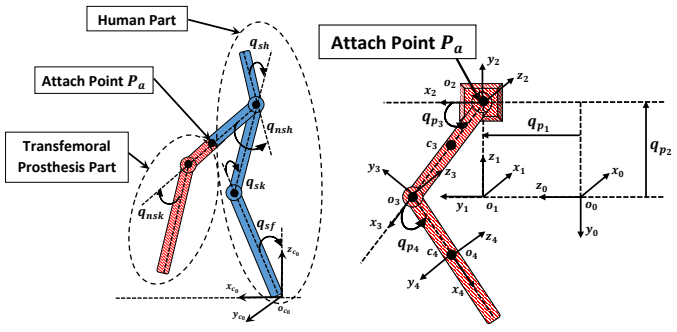

(a) (b)

Fig. 1: (a) Combined human-prosthesis system, (b) Transfemoral prosthesis system

A. Robust Sliding Mode Controller

An error vector s and signal vector v, which are n-element vectors, are defined as [27]

$$s = \dot{e} + \lambda e \qquad v = \dot{q}_p^d - \lambda e \tag{3}$$
$$e = q_p - q_p^d \qquad \lambda = \mathrm{diag}(\lambda_1, \lambda_2, ..., \lambda_n), \lambda_i > 0$$

Using the linearity of the parameters and definition of v in Eq. (3), the left hand side of Eq. (2) can be written as

$$M_p(q_p)\ddot{q}_p + C_p(q_p, \dot{q}_p)\dot{q}_p + g_p(q_p) = Y(q_p, \dot{q}_p, v, \dot{v})p \tag{4}$$

where $Y(q_p, \dot{q}_p, v, \dot{v}) \in \Re^{n\times r}$ is an acceleration-free controller regressor; n is the number of prosthetic degrees of freedom; $p \in \Re^{r\times1}$ is a parameter vector.

The following control law is used to smooth control signal chattering, providing robustness to parameter uncertainties and unmodeled dynamics [28]:

$$\begin{aligned} u_p &= \hat{M}_p\dot{v} + \hat{C}_p v + \hat{g}_p - K_d\,\mathrm{sat}\,(s/\mathrm{diag}(\phi)) \\ &= Y(q_p, \dot{q}_p, v, \dot{v})\hat{p} - K_d\,\mathrm{sat}\,(s/\mathrm{diag}(\phi)) \end{aligned} \tag{5}$$

where $\hat{M}_p$, $\hat{C}_p$, and $\hat{g}_p$ are estimates of M_p, C_p, and g_p respectively; $K_d = \mathrm{diag}(K_{d1}, K_{d2}, ..., K_{dn}), K_{di} > 0$; ϕ is the width of the saturation function such that $\phi = \mathrm{diag}(\phi_1, \phi_2, ..., \phi_n), \phi_i > 0$. Note that the division and saturation operations for s and $\mathrm{diag}(\phi)$ in the term $\mathrm{sat}\,(s/\mathrm{diag}(\phi))$ are interpreted element-wise and $\mathrm{diag}(\phi)$ is an n-element vector. Substituting the control law of Eq. (5) into Eq. (2) and using Eq. (3) yields the following error dynamics:

$$\dot{s} = -M_p^{-1}\left(C_p s + K_d\,\mathrm{sat}(s/\mathrm{diag}(\phi)) + M_p^{-1}Y(q_p, \dot{q}_p, v, \dot{v})\tilde{p}\right. \tag{6}$$

where $\tilde{p} = \hat{p} - p$ is parameter estimation error. The addition of $\mathrm{sat}\,(s/\mathrm{diag}(\phi))$ in the above control law results in smoother control behavior in the boundary layer $|s| \le \mathrm{diag}(\phi)$.

Using the control law of Eq. (5), it can be shown that all error trajectories starting outside the boundary layer will be attracted by the layer while those which start inside the boundary layer will remain inside for all $t \ge 0$ (the boundary layer is an invariant set). For this purpose, a boundary layer trajectory is defined to measure the distance between the current s to the boundary layer [27]:

$$s_\Delta = \begin{cases} 0 & \text{if } |s| \le \mathrm{diag}(\phi) \\ s - \phi\,\mathrm{sat}\,(s/\mathrm{diag}(\phi)) & \text{if } |s| > \mathrm{diag}(\phi) \end{cases} \tag{7}$$

where s_Δ is a n-element vector; ϕ is the boundary layer thickness. The proposed control structure also satisfies the following reaching condition:

$$s_\Delta^T M_p \dot{s}_\Delta \le -\max(\gamma_i)\|s_\Delta\|_1 \tag{8}$$

where $\gamma = (\gamma_1, \gamma_2, ..., \gamma_n)$, $\gamma_i > 0$. To prove stability of the proposed controller, a scalar positive definite continuously-

differentiable Lyapunov function is considered, which is a function of $s_\triangle$

$$V(s_\triangle) = \frac{1}{2}\left(s_\triangle^T M_p s_\triangle\right) \tag{9}$$

Theorem 1: *Let assume that* $Y(q_p, \dot{q}_p, v, \dot{v})\tilde{p} \leq F$ *and define* $F_m = \max(F_i)$ *and* $\gamma_m = \max(\gamma_i)$. *Given the Lyapunov function* $V(s_\triangle)$ *of Eq. (9) and the RS controller* u_p *of Eq. (5), if* $K_d \geq F_m + \gamma_m - \kappa \dot{q}_{p_{max}} \phi$, *then* $\dot{V}(s_\triangle) \to 0$ *and* $s_\triangle \to 0$ *as* $t \to 0$ *for all* $p \in \Re^r$ *and* $s(0) \in \Re^n$, *which implies* $|s_i| \leq \phi_i$ *and the error term has the property that* $e \leq \phi_i/\lambda_i$.

Proof: Taking the derivative of Eq. (9), noting that $\dot{s}_\triangle = \dot{s}$ if starting outside the boundary layer, and substituting the error dynamic of Eq. (6) into Eq. (9) gives

$$\begin{aligned}\dot{V}(s_\triangle) = &-s_\triangle^T C_p s + \frac{1}{2}\left(s_\triangle^T \dot{M}_p s_\triangle\right) \\ &- s_\triangle^T K_d \,\mathrm{sat}\left(s/\mathrm{diag}(\phi)\right) + s_\triangle^T Y(q_p, \dot{q}_p, v, \dot{v})\tilde{p}\end{aligned} \tag{10}$$

Substituting $s = s_\triangle + \phi\,\mathrm{sat}\left(s/\mathrm{diag}(\phi)\right)$ from Eq. (7) into Eq. (10) if starting outside the boundary layer, and using the skew symmetric property $\left(s_\triangle^T(\dot{M}_p - 2C_p)s_\triangle = 0\right)$ yields [29], [30]:

$$\dot{V}(s_\triangle) = -s_\triangle^T(C_p\phi + K_d)\mathrm{sat}\left(s/\mathrm{diag}(\phi)\right) + s_\triangle^T Y(q_p, \dot{q}_p, v, \dot{v})\tilde{p} \tag{11}$$

Tuning K_d and ϕ so $C_p\phi + K_d \geq K_m I$ (K_m is a positive scalar), and noting that $s_\triangle^T \mathrm{sat}\left(s/\mathrm{diag}(\phi)\right) = \|s_\triangle\|_1$ gives

$$\dot{V}(s_\triangle) \leq -K_m\|s_\triangle\|_1 + s_\triangle^T Y(q_p, \dot{q}_p, v, \dot{v})\tilde{p} \tag{12}$$

Defining $K_m = F_m + \gamma_m$, where $K_m = \max(K_{di})$ and noting that $s_\triangle^T F$ is upper bounded by $F_m\|s_\triangle\|_1$ yields

$$\dot{V}(s_\triangle) \leq -\gamma_m\|s_\triangle\|_1 \tag{13}$$

Therefore, if error trajectories start outside the boundary layer, $\dot{V}(s_\triangle) \to 0 \Rightarrow s_\triangle \to 0$ in a finite time less than $s_i(0)/\gamma_i$. In turn, the distance between s and the boundary layer approaches zero, showing that s is attracted by the boundary layer. This result implies that $|s_i| \leq \phi_i$ and $e \leq \phi_i/\lambda_i$ proving stability of the prosthesis / RS controller combination and boundedness of the tracking error trajectories by the boundary layer (regardless of starting point). It should also be noted that since C_p is upper bounded by $\kappa\|\dot{q}_p\|$ and $\|\dot{q}_p\| \leq \dot{q}_{p_{max}}$, such that $K_d \geq K_m - \kappa\dot{q}_{p_{max}}\phi$, $\dot{V}(s_\triangle) \to 0$ as $t \to 0$. □

B. Robust Passivity Controller

With the definition of error and signal vectors from Eq. (3) and acceleration-free controller regressor from Eq. (4), the robust passivity-based control law is presented as [31]:

$$u_p = Y(q_p, \dot{q}_p, v, \dot{v})\hat{p} - K_d s \tag{14}$$

Substituting Eqs. (3) and (14) into Eq. (2), and defining $\hat{p} = p_0 + u_b$ and $\tilde{p} = p_0 - p$ yields the error dynamics

$$\dot{s} = -M_p^{-1}\left(C_p s + K_d s\right) + M_p^{-1} Y(q_p, \dot{q}_p, v, \dot{v})(\tilde{p} + u_b) \tag{15}$$

where p_0 is the nominal parameter vector, $\|\tilde{p}\| \leq \rho$, $\rho \geq 0$, and auxiliary control term u_b can be defined as [31]

$$u_b = \begin{cases} -\rho r/\|r\| & ,\text{if } \|r\| > \epsilon \\ -\rho r/\epsilon & ,\text{if } \|r\| \leq \epsilon \end{cases} \tag{16}$$

where $r = Y^T(q_p, \dot{q}_p, v, \dot{v})s$. Consider the following scalar positive definite Lyapunov function as a function of s:

$$V(s, e) = \frac{1}{2}\left(s^T M_p s + e^T \lambda K_d e\right) \tag{17}$$

Theorem 2: *Let* Q *be* $\mathrm{diag}(\lambda^T K_d \lambda, K_d)$. *Given the Lyapunov function* $V(s, e)$ *of Eq. (17), the RP controller* u_p *of Eq. (14), and the auxiliary control term* u_b *of Eq. (16), if* $\|r\| > \epsilon$, *or* $\|r\| \leq \epsilon$ *and the error term has the property that* $\|e\| \geq \sqrt{\rho\epsilon/2\lambda_{\min}(Q)}$, *then* $\dot{V}(s, e) \to 0$ *as* $t \to 0$ *for all* $\tilde{p} \in \Re^r$, *which implies boundedness of all tracking error trajectories.*

Proof: Taking the derivative of Eq. (17), substituting the error dynamics of Eq. (15), and using the skew symmetric property $\left(s^T(\dot{M}_p - 2C_p)s = 0\right)$ gives

$$\dot{V}(s, e) = s^T Y(q_p, \dot{q}_p, v, \dot{v})(\tilde{p} + u_b) - e^T\lambda^T K_d \lambda e - \dot{e}^T K_d \dot{e} \tag{18}$$

Using the definition of r yields

$$\dot{V}(s, e) = r^T(\tilde{p} + u_b) - e^T Q e \tag{19}$$

If $\|r\| > \epsilon, \quad u_b = -\rho r/\|r\|$ and

$$\dot{V}(s, e) \leq \|r\|\tilde{p} - \rho\|r\| - e^T Q e \tag{20}$$

and it can be concluded that $\dot{V}(s, e) < 0$ using the Cauchy-Schwartz inequality ($\|r\|(\tilde{p} - p) \leq 0$). On the other hand, if $\|r\| \leq \epsilon, \quad u_b = -\rho r/\epsilon$ and

$$\dot{V}(s, e) \leq \|r\|\tilde{p} - \rho\|r\|^2/\epsilon - e^T Q e \tag{21}$$

Noting that $\|r\|\tilde{p} - \rho\|r\|^2/\epsilon$ is upper bounded by $\rho\epsilon/2$, $\dot{V}(s, e) < 0$ if

$$e^T Q e > \rho\epsilon/2 \tag{22}$$

As $e^T Q e$ is upper bounded by $\lambda_{\max}(Q)\|e\|^2$ and lower bounded by $\lambda_{\min}(Q)\|e\|^2$, the condition of Eq. (22) can be rewritten as

$$\|e\| \geq \sqrt{\frac{\rho\epsilon}{2\lambda_{\min}(Q)}} \tag{23}$$

Therefore, using the control law of Eq. (14), the term $r^T(\tilde{p} + u_b)$ in Eq. (19) is forced to be non-negative, regardless of the lack of information on $\tilde{p}$, which results in $\dot{V}(s, e) < 0$. That is, the prosthesis / RP controller emulates humanlike walking with the bounded tracking error trajectories. □

IV. PROSTHESIS CONTROLLERS SIMULATION RESULTS

In this section, the effectivenesses of the proposed RS and RP controllers are demonstrated by performing simulation studies on the combined human-prosthesis model, while supplying the controllers with only the prosthesis model information from Section II. As mentioned above, the

proposed controllers of Section III are used to control the transfemoral prosthesis shown in Fig. 1 (i.e., prosthetic knee joint), and the rest of the joints are controlled by the feedback linearization human-inspired controller [26]. The RS and RP controllers are then compared to each other with regard to tracking performance and robustness to unexpected push and obstacle disturbances.

A. Tracking Performance and Humanlike Walking

The reference gait is obtained from the optimization problem in Section II, yielding desired trajectories y_d, q_c, and q_p for the controllers. It is assumed that both human and prosthetic parameters are unknown to the controller, the prosthetic ankle is underactuated, and the healthy ankle can be actuated by the amputee. See Fig. 4a.

Fig. 2 shows tracking performances of the prosthetic knee during swing and stance phases for both RS and RP controllers. It can be seen that both controllers track the desired trajectories in both stance and non-stance phase. While the healthy human walking gait demonstrates roughly equal stance and swing phase durations, differences can arise from inherent asymmetries in the hybrid system. As mentioned in Section II, the human ankle remains actuated and able to inject energy into the system during human stance, while the passive prosthetic ankle is unable to do so. This discrepancy results in a shorter prosthesis swing than prosthesis stance (as shown in Fig. 2).

Table I lists RMSE values for prosthetic knee tracking using both RS and RP controllers in stance and swing phases. This table shows that RS controller provides poorer tracking during both stance and swing phases. Tracking for 40 steps yields $\mathrm{RMSE}_{\mathrm{RS}} = 0.0124$ rad and $\mathrm{RMSE}_{\mathrm{RP}} = 0.0064$ rad showing that in general, the RP controller outperforms the RS controller with regard to prosthetic knee tracking.

Fig. 3 show phase portraits of the stance and non-stance knee joints for both RS and RP controllers over 40 steps.

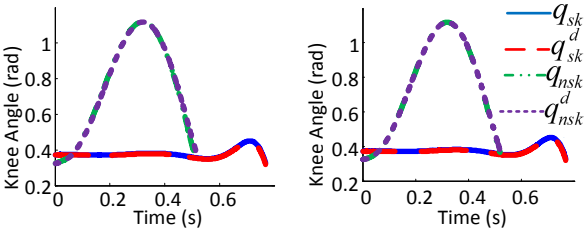

(a) RS controller (b) RP controller

Fig. 2: Tracking performance of the knee joint for different controllers

TABLE I: Tracking results for RS and RP controllers. The best value for each metric is underlined.

	RS	RP
$\mathrm{RMSE}_{\mathrm{Stance}}$ (rad)	0.0070	<u>0.0037</u>
$\mathrm{RMSE}_{\mathrm{Swing}}$ (rad)	0.0120	<u>0.0066</u>
$\mathrm{RMSE}_{\mathrm{40Steps}}$ (rad)	0.0124	<u>0.0064</u>

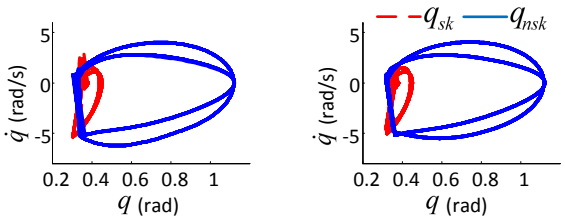

(a) RS controller (b) RP controller

Fig. 3: Phase portrait of the knee joint over 40 steps for both controllers

The resulting portraits demonstrate convergence to a stable limit periodic orbit while applying a feedback linearization human-inspired controller to the rest of the system. It can also be seen that the impact upon foot strike induces a larger knee velocity change using the RS controller than the RP controller, resulting in a larger velocity jump when the stance knee angle is 0.35 rad for the RS controller.

B. Robustness Tests

To test walking system stability and quantify human-prosthesis system robustness in the presence of disturbances (unexpected push and obstacle as shown in Fig. 4b), two robustness tests for both proposed controllers are performed. For the first robustness test, both x-direction and z-direction (with respect to the combined system world frame $O_{co} = \{x_{co}, y_{co}, z_{co}\}$ shown in Fig. 4b) pushes are applied to the prosthetic leg.

1) Robustness to Impulse Force: For the first test, an x-direction impulse (lasting for 0.01 sec) is applied to the prosthesis under RS control for 40 steps each time it begins to swing forward. The force of the impulse is iteratively increased with a resolution of 1 N until simulation failure. The maximum tolerated force was determined to be 60 N. Fig. 5a depicts the phase portrait of the system under RS control during the test. It can be observed that the non-stance knee phase portrait deviates when the x-direction force is applied, but then smoothly converges to the cycle. This implies that the RS controller can consistently tolerate the applied x-direction disturbance.

A similar test is also performed for the RP controller, but this controller is not able to tolerate the same 60 N force

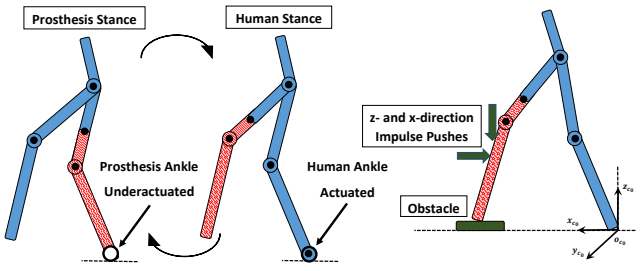

(a) (b)

Fig. 4: (a) Two-domain hybrid asymmetric human-prosthesis system (b) Robustness test with push and obstacle disturbances

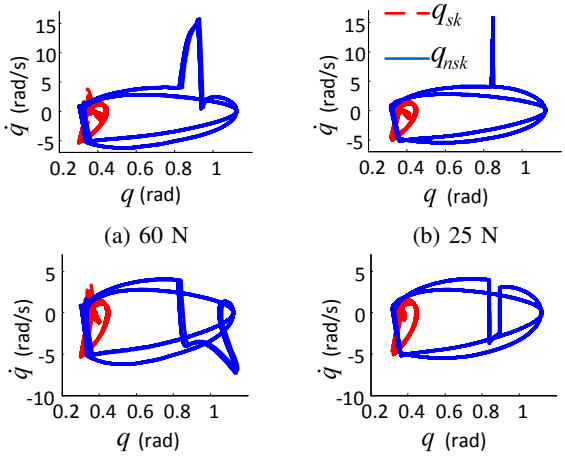

(a) 60 N (b) 25 N

(c) 30 N (d) 3 N

Fig. 5: Phase portrait of the knee joint over 40 steps with the applied impulse force: (a) RS controller with x-direction push, (b) RP controller with x-direction push, (c) RS controller with z-direction push, (d) RP controller with z-direction push

in the x-direction, causing the walking system to fall after 10 steps. However, Fig. 5b shows convergence of the RP controller phase portrait to the cycle after reducing the force to 25 N during each prosthetic swing.

Similarly, a 30 N z-direction force is applied during prosthetic swing for both controllers for 40 steps. The RS controller shows a good robustness to this force by completing 40 steps, while simulation with the RP controller fails again. Fig. 5c and 5d demonstrate convergence of both controllers to the cycle when the z-direction force applied to the RP controller is reduced to 3 N. Fig. 5 also shows a sharper velocity change on the phase portrait of the RP controller compared to the RS controller when z- and x-direction forces are applied to the prosthetic leg.

2) Robustness to Obstacles: For the second robustness test, the human-prosthesis system is forced to walk over a 20 mm obstacle for 40 steps. Fig. 6a demonstrates the first two steps of the actual and desired prosthesis knee angles for both RS and RP controllers when an unexpected obstacle appears during the prosthesis stance phase (obstacle appears at the first prosthesis stance). From this figure, it is seen that both controllers can overcome the obstacle, while their next swing steps tend toward greater knee extension.

To better characterize the controller responses, Fig. 6a is zoomed in at the moment the obstacle is encountered, shown in Fig. 6b. From this figure, it is easily observed that both RS and RP controllers quickly converge to the desired trajectory after meeting the obstacle, while the RP controller has a relatively more sluggish response. Table II presents the robustness performance of both proposed controllers.

In general, as seen from tracking results and robustness tests, the RS controller provides better robustness and stability in the presence of disturbances, while the RP controller has better tracking performance.

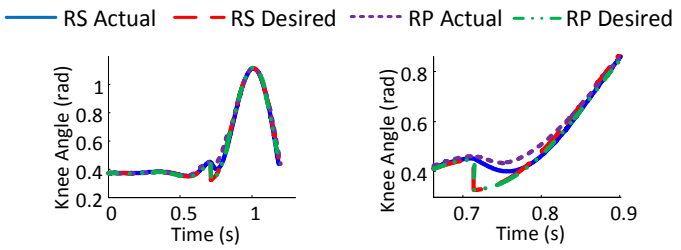

(a) (b)

Fig. 6: Prosthetic knee angle when the system walks over the obstacle

TABLE II: Robustness performance for RS and RP controllers, where MDT is maximum disturbance tolerated by the controller. The better value for each metrics is underlined.

	RS	RP
$\text{MDT}_{\text{Force}_x}$ (N)	<u>60</u>	25
$\text{MDT}_{\text{Force}_z}$ (N)	<u>30</u>	3
$\text{MDT}_{\text{Obstacle}}$ (mm)	<u>20</u>	<u>20</u>

V. EXPERIMENTAL IMPLEMENTATION AND RESULTS

A. AMPRO3 Implementation

In this section, the RS and RP controllers are implemented experimentally on the powered custom-built self-contained transfemoral prosthesis AMPRO3, as shown in Fig. 7a [24]. This device can be actuated at both knee and ankle joints in the sagittal plane with a pair of torsion springs between the gearbox and joints, resulting in series elastic actuators (SEA). AMPRO3 also uses two relative incremental encoders at both knee and ankle joints. A 6-axis load cell is located right below the ankle joint to measure the ground reaction force (GRF), using the information to determine current gait state. An attached knee adaptor, or bypass, allows able-bodied human subjects to use the device for walking; see Fig. 7b. The scope of this study only aims to control the prosthesis knee joint, and as such, the prosthetic ankle is treated as a passive joint.

High-level controllers and trajectories are implemented in C++, organized as Robot Operating System (ROS) packages. A single Beaglebone Black (BBB) calculates trajectory and controller outputs at 200 Hz.

B. Experimental Results

In Section IV, both RS and RP controllers were validated in tracking and robustness, and a comparison was performed. Now, the proposed controllers are tested on AMPRO3 with an able-bodied test subject. During the experiments, the prosthesis knee joint is controlled with the proposed RS and RP controllers, while the ankle behaves passively to emulate the point foot conditions used during simulation. A simple PD controller with low value coefficients for the ankle is employed with the goal of modeling the prosthetic ankle as a passive spring-damper mechanism during locomotion (i.e., small rotation of the ankle).

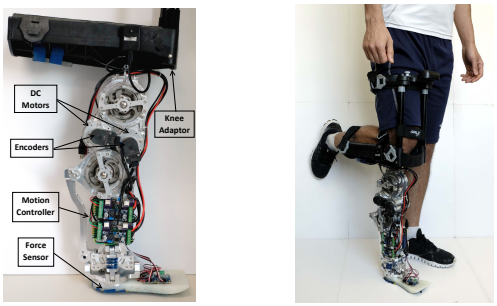

(a) (b)

Fig. 7: (a) AMPRO3 device, (b) Human test subject wearing AMPRO3

For each controller, the healthy human test subject is instructed to walk for 2.5 min with the prosthesis at a treadmill speed of 2 mph. Fig. 8a and 8b show tracking performance of RS and RP controllers respectively at time window $t \in [100, 104]$ sec. From Fig. 8, it is observed that both controllers achieve tracking of the prosthesis knee joint, providing a humanlike gait. However, the RP controller yields better knee angle tracking compared to the RS controller ($\mathrm{RMSE}_{\mathrm{RP}} = 0.0221$ rad versus $\mathrm{RMSE}_{\mathrm{RS}} = 0.0305$ rad) for 2.5 min of walking.

Fig. 9 demonstrates phase portraits of the prosthetic knee joint using RS and RP controllers for 2.5 min of walking. This figure shows a stable limit cycle of the prosthesis for both proposed controllers, indicating stable walking gaits.

Figs. 10a and 10b shows gait tiles of human-prosthesis walking in simulation and AMPRO3 walking with an able-bodied human test subject over two steps using RS and RP controllers respectively. These figures visually show humanlike walking for both proposed controllers. In addition, AMPRO3 walking results using the proposed RS and RP controllers in this paper can be seen in a video available at [32].

Fig. 11 compares prosthetic knee torques for RS and RP controllers for $t \in [100, 104]$ sec. It can be seen that the RS controller generates fewer velocity sign changes during walking and lower absolute peak torque values at the end of swing. These observations correlate with the test subject's perception of walking to be smoother and better while using the RS controller.

Table III lists maximum torque values $\tau_{\max}$, maximum tracking error $E_{\max}$, and RMSE for AMPRO3 using the proposed RS and RP controllers over 2.5 min of walking. Better values for each metric are underlined in the table, demonstrating that the RS controller decreases maximum prosthetic knee torque by 27% compared to RP controller, whereas the RP controller reduces maximum knee tracking error by 33% and improves RMSE by 27% compared to the RS controller.

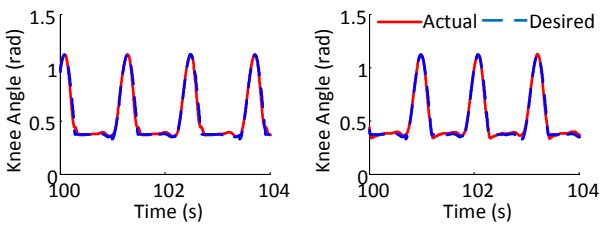

(a) RS controller (b) RP controller

Fig. 8: Experimental tracking performance of the prosthetic knee joint using different controllers

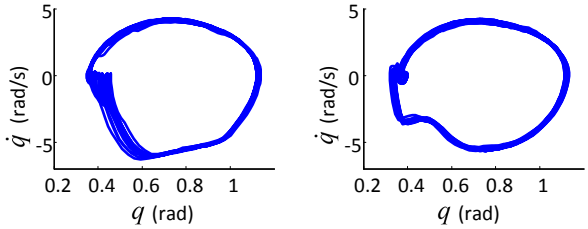

(a) RS controller (b) RP controller

Fig. 9: Experimental phase portrait of the prosthetic knee joint for 2.5 min of walking with different controllers

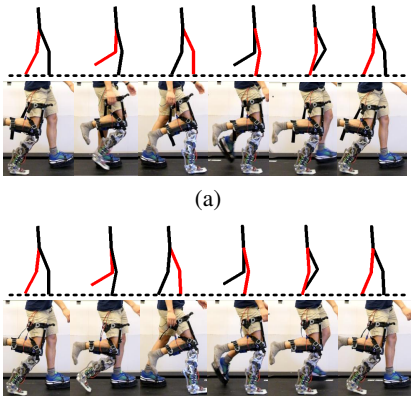

(a)

(b)

Fig. 10: Gait tiles of human-prosthesis walking in simulation and AMPRO3 walking with an able-bodied human test subject in experiment over two steps using (a) RS control and (b) RP control

VI. CONCLUSIONS AND FUTURE WORK

This paper presented, compared, and experimentally tested two robust model-based controllers, RS and RP, for the newly designed powered transfemoral prosthesis AMPRO3. Compared to traditional impedance controllers, there were no concerns regarding correct step cycle division and tedious parameter tuning. Stability and robustness of the proposed controllers were evaluated mathematically and via simulation.

Simulations on the human-prosthesis model (with the assumption of underactuated prosthetic ankle) for the proposed controllers showed that both controllers provided good prosthetic knee tracking performance, good robustness against disturbances, and humanlike walking. Both proposed controllers were experimentally verified on AMPRO3 (with passive ankle) using an able-bodied human test subject, again yielding good tracking and reasonable prosthetic knee torque.

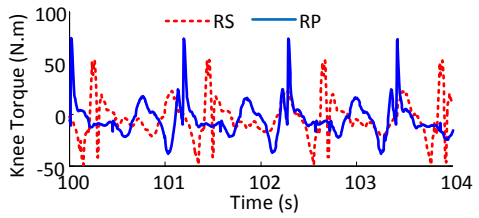

Fig. 11: Experimental prosthetic knee torque comparison between RS and RP controllers

TABLE III: Experimental results of AMPRO3 using RS and RP controllers. Better values for each metric are underlined.

	RS	RP
$\tau_{\max}$ (N.m)	54	74
RMSE (rad)	0.0305	0.0221
$E_{\max}$ (rad)	0.1180	0.0785

Experimental results showed that the RS controller decreased maximum prosthetic knee torque by 27% compared to the RP controller, whereas the RP controller reduced maximum knee tracking error value by 33% and improved RMSE value by 27% compared to the RS controller.

From both simulation and experimental results, it was found that the RS controller rendered better robustness and stability in the presence of disturbances, smoother walking, and lower absolute peak torque compared to the RP controller. Conversely, the RP controller provided better tracking for the prosthetic knee joint.

In terms of future work, both robust and adaptive controllers will be applied to both joints of the powered prosthesis AMPRO3, thereby fully utilizing its actuation abilities. There are open questions related to the energy cost, subjective perception of the quality of walking, and robustness of fully actuated prosthetic walking with both controllers.

REFERENCES

[1] T. Dillingham *et al.*, "Limb amputation and limb deficiency: epidemiology and recent trends in the united states," *Southern Medical Journal*, vol. 95, no. 8, pp. 875–884, 2002.

[2] K. Inoue, T. Tanaka, T. Wada, and S. Tachiwana, "Development of a passive knee mechanism that realizes level walk and stair ascent functions for transfemoral prosthesis," in *IEEE International Conference on Biomedical Robotics and Biomechatronics*, (Singapore), 2016.

[3] B. G. A. Lambrecht and H. Kazerooni, "Design of a semi-active knee prosthesis," in *IEEE International Conference on Robotics and Automation*, (Kobe), 2009.

[4] F. Sup, H. A. Varol, and M. Goldfarb, "Upslope walking with a powered knee and ankle prosthesis: initial results with an amputee subject," *IEEE transactions on neural systems and rehabilitation engineering*, vol. 19, no. 1, pp. 71–78, 2011.

[5] D. A. Winter, *The biomechanics and motor control of human gait: normal, elderly, and pathological*. University of Waterloo Press, 1991.

[6] B. E. Lawson, H. A. Varol, and M. Goldfarb, "Standing stability enhancement with an intelligent powered transfemoral prosthesis," *IEEE Transactions on Biomedical Engineering*, vol. 58, no. 9, pp. 2617–2624, 2011.

[7] R. D. Gregg and J. W. Sensinger, "Towards biomimetic virtual constraint control of a powered prosthetic leg," *IEEE Transactions on Control Systems Technology*, vol. 22, no. 1, pp. 246–254, 2014.

[8] K. Fite, J. Mitchell, F. Sup, and M. Goldfarb, "Design and control of an electrically powered knee prosthesis," in *IEEE International Conference on Rehabilitation Robotics*, (Noordwijk), 2007.

[9] F. Sup, A. Bohara, and M. Goldfarb, "Design and control of a powered transfemoral prosthesis," *International journal of robotics research*, vol. 27, no. 2, pp. 263–273, 2008.

[10] N. Fey, A. Simon, A. Young, and L. Hargrove, "Ucontrolling knee swing initiation and ankle plantarflexion with an active prosthesis on level and inclined surfaces at variable walking speeds," *IEEE Journal of Translational Engineering in Health and Medicine*, vol. 2, pp. 1–12, 20104.

[11] S. Au, M. Berniker, and H. Herr, "Powered ankle-foot prosthesis to assist level-ground and stair-descent gaits," *Journal of Surgical Orthopedic Advances*, vol. 21, no. 4, pp. 654–666, 2008.

[12] K. Hollander and T. Sugar, "A robust control concept for robotic ankle gait assistance," in *IEEE* 10^{th} *International Conference on Rehabilitation Robotics*, (Noordwijk, Netherlands), 2007.

[13] C. G. Atkeson and S. Schaal, "Robot learning from demonstration," *ICML*, vol. 97, pp. 12–20, 1997.

[14] J. Nakanishi *et al.*, "Learning from demonstration and adaptation of biped locomotion," *Robotics and Autonomous Systems*, vol. 47, no. 2, pp. 79–91, 2004.

[15] A. M. Simon *et al.*, "Configuring a powered knee and ankle prosthesis for transfemoral amputees within five specific ambulation modes," *PloS one*, vol. 9, no. 6, p. e99387, 2014.

[16] H. Zhao, S. Kolathaya, and A. D. Ames, "Quadratic programming and impedance control for transfemoral prosthesis," in *IEEE International Conference on Robotics and Automation*, (Hong Kong, China), 2014.

[17] H. Zhao, J. Horn, J. Reher, V. Paredes, and A. D. Ames, "First steps toward translating robotic walking to prostheses: a nonlinear optimization based control approach," *Autonomous Robots*, vol. 19, no. 1, pp. 1–18, 2011.

[18] H. Zhao, J. Reher, J. Horn, V. Paredes, and A. D. Ames, "Realization of nonlinear real-time optimization based controllers on self-contained transfemoral prosthesis," in *IEEE/ACM International Conference on Cyber Physics System*, (Seattle, WA), 2015.

[19] J. Hu, J. Pratt, C.-M. Chew, H. Herr, and G. Pratt, "Adaptive virtual model control of a bipedal walking robot," in *IEEE International Joint Symposia on Intelligence and Systems*, (Rockville, MD), 1998.

[20] Q. Nguyen and K. Sreenath, "l_1 adaptive control for bipedal robots with control lyapunov function based quadratic programs," in *American Control Conference*, (Chicago, IL), 2015.

[21] S. C. Hsu, X. Xu, and A. D. Ames, "Control barrier function based quadratic programs with application to bipedal robotic walking," in *American Control Conference*, (Chicago, IL), 2015.

[22] M. Moosavi, S. A. Fakoorian, V. Azimi, H. Richter, and D. Simon, "Derivative-free kalman filtering-based control of prosthetic legs," in *Submitted to American Control Conference*, (Seattle, WA), 2017.

[23] M. Sharifi, S. Behzadipour, and G. Vossoughi, "Nonlinear model reference adaptive impedance control for humanrobot interactions," *Control Engineering Practice*, vol. 32, no. 8, pp. 9–27, 2014.

[24] H. Zhao, A. Hereid, E. Ambrose, and A. D. Ames, "3d multi-contact gait design for prostheses: hybrid system models, virtual constraints and two-step direct collocation," in *Conference on decision and control*, (Las Vegas, NV), 2016.

[25] A. D. Ames, "Human-inspired control of bipedal walking robots," *IEEE Transactions on Automatic Control*, vol. 59, no. 5, pp. 1115–1130, 2014.

[26] A. D. Ames, "First steps toward automatically generating bipedal robotic walking from human data," *Robotic Motion and Control*, vol. 422, 2011.

[27] J.-J. E. Slotine and J. A. Coetsee, "Adaptive sliding controller synthesis for non-linear systems," *International Journal of Control*, vol. 43, no. 6, pp. 1631–1651, 1984.

[28] J.-J. E. Slotine and W. Li, *Applied nonlinear control*. NJ: Prentice-Hall, 1991.

[29] V. Azimi, D. Simon, and H. Richter, "Stable robust adaptive impedance control of a prosthetic leg," in *Proceedings of the ASME Dynamic Systems and Control Conference*, (Columbus, OH), 2015.

[30] V. Azimi, D. Simon, H. Richter, and S. A. Fakoorian, "Robust composite adaptive transfemoral prosthesis control with non-scalar boundary layer trajectories," in *Proceedings of the American Control Conference*, (Boston, MA), 2016.

[31] M. Spong, S. Hutchinson, and M. Vidyasagar, *Robot Modeling and Control*. Wiley, 2005.

[32] Experimental and simulation results: https://www.youtube.com/watch?v=Aq8_H_nSAxI